SPATIAL ATTENUATION PREDICTION OF LAMB WAVES IN COMPOSITE MATERIALS

SHUANGLIN GUO[*], MARC REBILLAT[*] AND NAZIH MECHBAL[*]

[*] Procédés et Ingénierie en Mécanique et Matériaux (PIMM)
ENSAM-CNAM-CNRS-HESAM
e-mail: shuanglin.guo@ensam.eu

Key words: Structural heath monitoring, Lamb wave, attenuation prediction, composite materials, viscoelastic damping.

Abstract. The inspection and detection of damage in composite materials using Lamb waves are particularly effective because Lamb wave can propagate over relatively large distance and hence can cover a large area with few testing time and equipment. However, comparing to the dispersion features that have been investigated systematically in the literature, predicting simply and reliably the spatial attenuation, which is the decrease of the amplitude of the propagating wave with distance, is still a challenge especially for structures large enough to industrial scale. In this paper, a simple model able to predict Lamb wave attenuation for different frequencies, which takes three damping models, Hysteretic, Kelvin-Voigt and Biot models into account, is derived directly from dispersion equations. Experiments on a practical aeronautical component, a Fan Cowl Structure, are carried out to validate the developed model. The merits of the proposed method lie in the fact that it is derived directly from dispersion equations instead of relying on complex finite element models and are thus simple to compute. Despite its simplicity, it is still effective when predicting attenuation coefficient for geometrically complex structures such as the Fan Cowl Structure.

1 INTRODUCTION

One of the most important issues in engineering concerns the monitoring and the early detection and localization of structural damages in order to prevent catastrophic failures. This process is referred to as Structural Health Monitoring (SHM) and is expected to provide considerable improvements with respect to safety and maintenance costs. Over half a century, modern SHM techniques have attained maturity in engineering practice, playing a significant role in evaluating the integrity and durability of engineered structures and assets [1]. With efficient, continuous and automated SHM techniques it is possible to identify structural damage at an early stage so as to prevent further failure occurring, producing huge economic and human benefit [2]. A SHM system generally focuses on three aspects: i) identifying the existence, location and classification of damage, ii) evaluating the severity of damage and iii) predicting the residual service life of structure.

Monitoring the health and integrity of complex aeronautical structures at the operation condition is mandatory. Among all kinds of SHM techniques, ultrasonic wave strategy based on Lamb waves is particularly effective in accomplishing this task because Lamb waves are able to propagate over relatively large distances and thus can cover a large with short testing time and few sensors. This benefit results in reduced labor and time to perform a test, and

makes long range inspection possible [3].

The dispersion and attenuation property of Lamb wave are two essential factors that need to be considered carefully when inspecting a structure by means of Lamb waves. Contrasting with dispersion which is the velocity change with frequency and that has already received sound exploration over the past decades, understanding and modeling the attenuation of Lamb wave in composite materials is still an open challenge. Existing efforts are limited to simulation and small-scale experiments. Recently, the damping effect on dispersion curves in plates was investigated theoretically [4]. The theoretical model to calculate the attenuation coefficient in viscoelastic anisotropic lamina was established based on linear 3D elasticity [5]. Two alternatives for this purpose were achieved via semi-analytical finite element method [6] and spectral collocation method [7]. The Rayleigh damping model was adopted to investigate the attenuated Lamb wave propagation in composite structures [8,9]. This model was also adopted to investigate damage detection of composite structures [10].

However, the investigation of Lamb wave attenuation in practical aeronautical structures caused by viscoelastic damping has been scarcely studied after the authors made an overall literature survey. This is owing to the complicated service conditions of aeronautical structures, including complex geometry and boundary of the structure itself, varying environment temperature and noise contamination etc. However, knowledge of in situ attenuation of Lamb waves for these structures is very desirable to deploy SHM strategies to monitor them. To solve this issue, this paper establishes a predictive model of Lamb wave attenuation for practical aeronautical structures and the experiment on a large-scale structure has been conducted to validate the model. Being able to predict spatial attenuation in such complex aeronautic structures paves the way for potential applications such as transducer network design optimization and amplitude-based damage localization algorithms development.

2 PREDICTIVE MODEL OF LAMB WAVE ATTENUATION

2.1 Attenuation representation of Lamb wave

When a Lamb wave mode is excited and propagates in a thin plate with infinite width, the displacement formula of the plate along the propagation direction can be expressed as follows [1].

$$u_x(x,t) = Ae^{j(kx-\omega t)} \tag{1}$$

where, A is the amplitude of wave at the origin point in temporal and spatial domain; k and ω are wavenumber and circular frequency respectively; x and t are the sensing distance and wave propagation time respectively; $j = \sqrt{-1}$.

It is supposed that as long as damping is considered the wavenumber is complex-valued,

$$k^* = k_r + jk_i \tag{2}$$

where, both k_r and k_i are real positive number. The superscript "*" denotes that the term correlated belongs to complex numbers space in this paper.

Substituting Eq. (2) into Eq. (1) can result in the following formula.

$$u_x(x,t) = Ae^{-k_i x}e^{j(k_r x-\omega t)} \tag{3}$$

Comparing Eq. (3) to Eq. (1), if the wavenumber is a complex number, the magnitude decays exponentially over the propagation distance, and this phenomenon is the so called

attenuation behavior of Lamb wave. Thus, k_i is defined as the attenuation coefficient in unit Np/m. Lamb wave attenuation is mainly caused by viscoelastic damping [6]. Hence, the damping models should be expounded firstly.

2.2 Damping effects on Lamb wave attenuation

There are generally two classical damping models to describe the viscoelasticity: Hysteretic (HR) model and Kelvin-Voigt (KV) model [11]. For both models, the Young modulus becomes a complex number E^* presented in Eqs. (4) and (5) respectively, in which the real part is defined as the storage modulus E representing the storage of energy and the imaginary part reflects the loss of energy. Besides the two models, a less common damping model named Biot (BT) model is used to investigate the damping effect on Lamb wave attenuation as presented in Eq. (6). This model is mainly applied to highly damped aerospace structures [12].

$$E^* = E(1 - j\gamma_{HR}) \quad \text{for Hystetetic model} \tag{4}$$

$$E^* = E\left(1 - j\gamma_{KV}\frac{f}{f_0}\right) \quad \text{for Kelvin} - \text{Voigt model} \tag{5}$$

$$E^* = E\left[1 + \frac{2}{\pi}\gamma_{BT}\ln\sqrt{1 + \left(\frac{2\pi f}{\epsilon}\right)^2} - j\frac{2}{\pi}\gamma_{BT}\arctan\left(\frac{2\pi f}{\epsilon}\right)\right] \quad \text{for Biot model} \tag{6}$$

where, γ_{HR}, γ_{KV} and γ_{BT} are the damping ratio for HR, KV and BT model respectively; ϵ is the scaling factor for BT model; f_0 is the reference frequency of KV model and it is set arbitrarily to be 250kHz in this paper. As this parameter is just a normalization parameter, setting arbitrarily its value is not an issue. If $\gamma_{KV} = \gamma_{HR}$ and $f = f_0$, KV model is equivalent to HR model at the frequency f_0 [11].

In light of the complex Young modulus, no matter which damping model being used, the classical dispersion equations become complex equations:

$$\begin{cases} \dfrac{\tan(\alpha_T^* h)}{\tan(\alpha_L^* h)} = -\dfrac{4k^2\alpha_L^*\alpha_T^*}{\left(\alpha_T^{*2} - k^2\right)^2} & \text{for symmetric modes} \\ \dfrac{\tan(\alpha_T^* h)}{\tan(\alpha_L^* h)} = -\dfrac{\left(\alpha_T^{*2} - k^2\right)^2}{4k^2\alpha_L^*\alpha_T^*} & \text{for anti} - \text{symmetric modes} \end{cases} \tag{7}$$

where, h is the half thickness of plate. $\alpha_L^* = \sqrt{\frac{\omega^2}{c_L^{*2}} - k^2}$ and $\alpha_T^* = \sqrt{\frac{\omega^2}{c_T^{*2}} - k^2}$; $c_L^* = \sqrt{\frac{\lambda^* + 2\mu^*}{\rho}}$ and $c_T^* = \sqrt{\frac{\mu^*}{\rho}}$ are the velocity of longitudinal and transverse mode respectively. $\lambda^* = \frac{E^*\nu}{(1+\nu)(1-2\nu)}$ and $\mu^* = \frac{E^*}{2(1+\nu)}$ are the Lame constants. ν and ρ are the Poisson ratio and density respectively.

The phase velocity c_p is the quotient between circular frequency and real wavenumber. The group velocity c_g is the partial derivative of circular frequency to real wavenumber.

$$c_p = \frac{\omega}{k_r} \tag{8}$$

$$c_g = \frac{\partial\omega}{\partial k_r} = \frac{c_p^2}{c_p - \omega\frac{dc_p}{d\omega}} \tag{9}$$

2.3 Numerical algorithm of predicting Lamb wave attenuation

The solution of the real-valued dispersion equation forms the dispersion curve, which is usually expressed as two pairs (ω, c_p) and (ω, k). However, the task of solving the complex dispersion equation is more complicated in the damped case because for the solution pair (ω, k^*) there are actually three real variables (ω, k_r, k_i) given that $k^* = k_r + jk_i$.

In order to overcome this issue, a two-step approach is proposed to work out the solution of the complex dispersion equation. In step 1, the solution pair (ω, k) for the real-valued equation $f(\omega, k) = 0$ is obtained, which can be easily achieved via many mature algorithms [13]. In step 2, the first three points of (ω, k^*) are acquired by directly solving the complex-valued equation $f^*(\omega, k^*) = 0$, during which the first three points of (ω, k) are taken as the initial guess because the real and complex solutions in (ω, k_r) plane mutually overlap at the initial stage of the dispersion curve. This is true since the effect of damping is relative low, such that $|k_i| \ll |k_r|$ and the strategy of searching the solutions of complex case in the neighborhood of the real case is working. For subsequent solutions, a curve tracing technique should be used in order to avoid branch crossing of different modes and thus guarantee a stable solution [13]. Specifically, the initial guess for the current solution is quadratically extrapolated from the previous three accurate solutions firstly, and then the current solution is obtained by directly solving the complex-valued dispersion equation. The presented two-step procedures form the numerical algorithm of predicting attenuation coefficient as summarized in Figure 1.

It should be noted that a strong complex equation solver is necessary for this algorithm. The authors hence employ the Levenberg–Marquardt based approach which is generally more efficient than Gauss-Newton method for solving a highly nonlinear equation to iteratively find the root of a complex equation from an initial guess [14].

3 DATA-DRIVEN BASED STRUCTURAL PARAMETERS ESTIMATION METHOD

It is evident from Figure 1 that in order to run the algorithm, the nine parameters should be provided in the first place. Normally, the thickness d, density ρ and reference frequency f_0 can be obtained easily. The other six parameters should be estimated from the collected Lamb wave signals, by which the group velocity and attenuation coefficient can be identified easily. Thus, the approach to identify the two parameters is described firstly.

3.1 Linear regression to identify group velocity and attenuation coefficient

3.1.1 Identification of group velocity

Under a specified frequency, a certain Lamb wave mode propagates in an isotropic plate or in an anisotropic plate but along a fixed direction with constant group velocity. Thus, the time-of-arrival (ToA) of Lamb wave is proportional to the sensing distance.

$$t_a = \frac{x}{c_g} + t_0 \tag{10}$$

where, t_a is the ToA; t_0 is the initial time of wave excited from actuator; x is the sensing distance; c_g is the group velocity for the propagating mode.

A series of t_a versus propagation distance x can be extracted from collected signals by indicating the time moment at the peak of the specified wave packet. If the scatter diagram

$(x_i, t_{a,i})$ is plotted, these scatter points should align with a straight line. Thus, linearly regressing these scatter points can be used to identify group velocity that is the inverse of the slope of the regressed line according to Eq. (10).

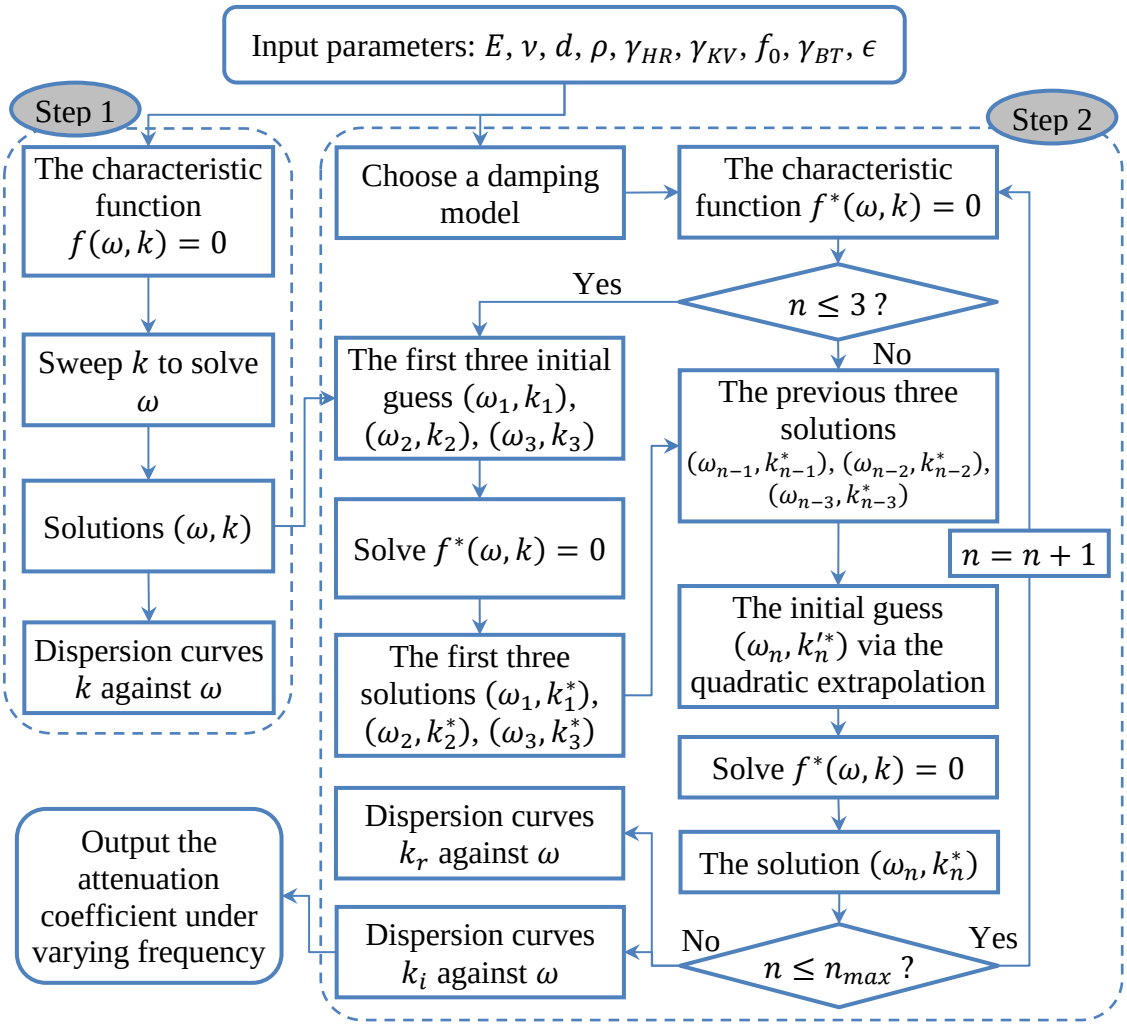

Figure 1: The flowchart of the numerical algorithm for predicting the attenuation coefficient

3.1.2 Identification of attenuation coefficient

Based on Eq. (3), the amplitude of wave exponentially decreasing over propagation distance is stated as following.

$$u_m = Ae^{-k_i x} \tag{11}$$

Making logarithm operation at two sides of Eq. (11) results in the linear formulation.

$$\ln u_m = -k_i x + \ln A \tag{12}$$

This equation manifests that the attenuation coefficient k_i can be identified from recorded signal by linearly regressing logarithmic amplitude of wave versus propagation distance, in which the attenuation coefficient is the negative of the slope of the regressed line.

3.2 The least square formulation for estimating material properties

The identified group velocity and attenuation coefficient can be used to estimate structural material properties.

3.2.1 Estimation of storage modulus and Poisson ratio

The theoretical group velocity that can be calculated from classical dispersion equations is expressed as the function with respect to storage modulus E and Poisson ratio ν if the frequency f is given.

$$c_g = G(E, \nu; f) \tag{13}$$

Once a series of group velocities under various frequencies are obtained from experiment, denoted as $(f_l, \tilde{c}_{g,l})$ $(l = 1,2,\cdots,m)$, the least square formulation can be used to estimate storage modulus and Poisson ratio.

$$\arg\min_{E,\nu} \sum_{l=1}^{m} \left[G(E, \nu; f_l) - \tilde{c}_{g,l}\right]^2 \tag{14}$$

where the symbol "$\tilde{}$" means that the variable it applies is extracted from experimental data. m is the number of excitation frequency during experiment.

3.2.2 Estimation of damping parameters

The theoretical attenuation coefficient k_i is expressed as the function with respect to a general damping parameter γ if the frequency f is given.

$$k_i = K(\gamma; f) \tag{15}$$

where, γ is γ_{HR}, γ_{KV} and γ_{BT}, ϵ for HR, KV and BT model respectively.

Therefore, if a series of attenuation coefficients under diverse frequencies are available from experiment, denoted as $(f_l, \tilde{k}_{i,l})$ $(l = 1,2,\cdots,m)$, the least square method can be also used to estimate the damping parameter respectively for the three damping models.

$$\arg\min_{\gamma} \sum_{l=1}^{m} \left[K(\gamma; f_l) - \tilde{k}_{i,l}\right]^2 \tag{16}$$

It should be noted that during performing the least square model of estimating damping parameters, the storage modulus and Poisson ratio estimated through Eq. (14) should be used. When all the required parameters are available, they can be inputted into the algorithm stated in Figure 1 to predict attenuation coefficient.

4 EXPERIMENTAL INVESTIGATION FOR A PRACTICAL AND GEOMETRICALLY COMPLEX AERONAUTICAL STRUCTURE

4.1 Experimental setup and signal presentation

A practical aeronautical structure, namely a fan cowl structure (FCS), is employed to validate the proposed Lamb wave attenuation coefficient prediction algorithm. The structure is made up of composite materials. Its thickness and density are 2.24mm and 1554kg/m^3 respectively. The geometry and transducers layout are shown in Figure 2. There are in total 13 piezoelectric lead zirconate titanate (PZT) transducers surface installed on the plate, among which PZT 1-6 and PZT 7-13 respectively align with an approximated straight line and are thus denoted as Group 2 and Group 3. Naturally, Group 1 includes all the PZTs. Since this

structure is large enough and a typical structure in aeronautical engineering, it is suitable for study the Lamb wave attenuation in composite plates.

During testing, input signal is chosen as a five-cycle sinusoid burst signal modulated by Hanning window. The central frequency varies from 50kHz to 250kHz with 5kHz increment. The signal from the function generator is passed through an amplifier for enlarging the voltage in order to produce Lamb wave signals powerful enough. In this experiment, the peak value of the excitation signal is $\pm 50V$. The actuator yields diverse Lamb wave modes and other sensors receive the signal. The data acquisition system (DAS) is adopted to collect signal and then stored in laptop for latter usage.

The sampling frequency is set to be 1MHz given that this value is the maximum capability of the DAS. In order to reduce noise, 10 repetition measurements are performed for each actuator excitation and then the 10 signals are processed with time averaging and wavelet denoising techniques. Figure 3 shows the typical Lamb wave signal in Group 2 in which PZT 1 serves as the actuator and its signal is normalized to the same magnitude of order than the receivers. It is evident that the signal amplitude decreases with the increasing of propagation distance.

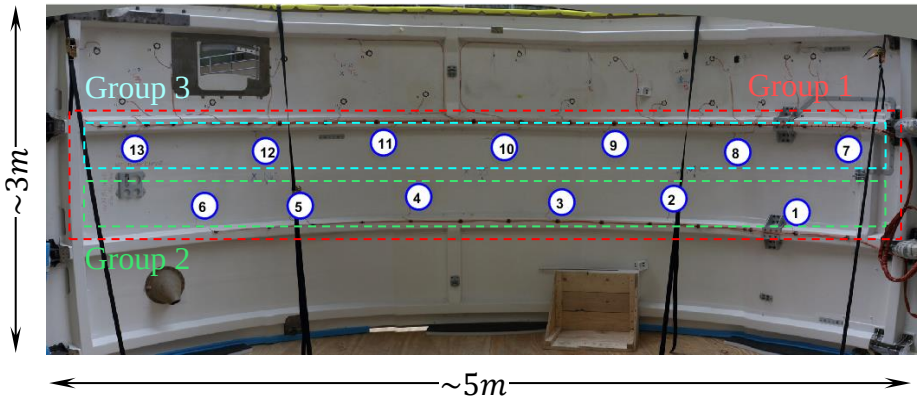

Figure 2: The FCS structure

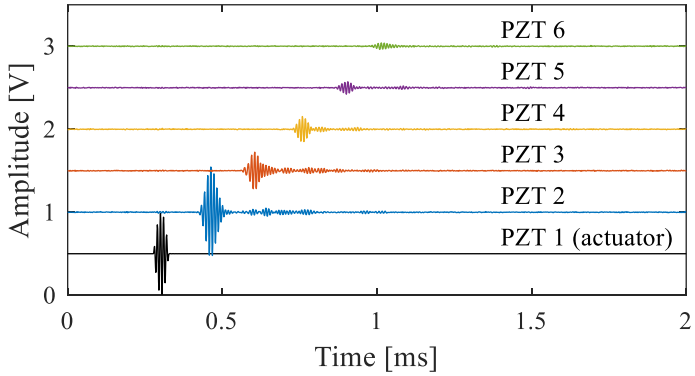

Figure 3: Typical Lamb wave signal (100kHz)

4.2 Dispersion curve identification for group velocity and attenuation coefficient

4.2.1 Group velocity and attenuation coefficient identification

The linear regression model described in section 3.1.1 is used to identify the group velocity at a given frequency. Taking the S0 mode of 100kHz as example, the experimentally measured scatter points between ToA and sensing distance are presented in Figure 4(a). The regressed lines for the three groups are also plotted based on these scatter points, for which the parameter $\alpha = 0.05$ is given to provide the confidence level (95%). In Table 1, the results including group velocity, the lower and upper bound of group velocity and the correlation coefficient of the three groups extracted from regression are listed. Combing Figure 4(a) and Table 1, it can be seen that the three kinds of sensor configuration produce pretty close group velocity identification result and meanwhile keep a very high correlation coefficient 0.99.

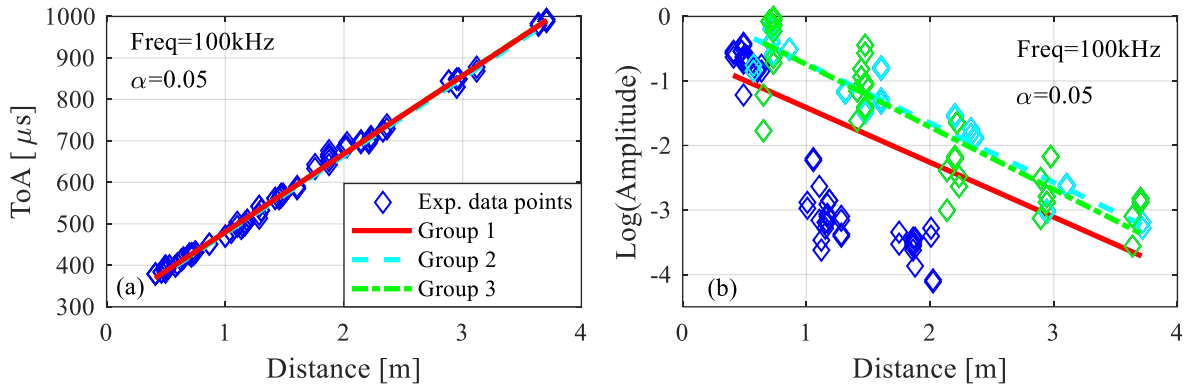

Figure 4: Example of (a) group velocity identification and (b) attenuation coefficient identification via linear regression method. In this figure, α is used to give the confidence level with $100(1-\alpha)\%$.

The same strategy is designed to identify attenuation coefficient in section 3.1.2. Like Figure 4(a), the linear regression process is illustrated in Figure 4(b) under the same frequency 100kHz. The results extracted from Figure 4(b) are presented in Table 2, from which the dispersed scatter points can be observed. This is due to the difficulty to exactly extract the peak value of S0 mode wave packet given the low sampling frequency (1MHz) and noise contamination. Moreover, the lower correlation coefficient of Group 1 (smaller than 0.6) manifests that the anisotropy of composite materials has an essential impact on attenuation since all propagation directions in Group 1 are mixed together whereas in Group 2 and 3, there exists only one main direction. Thus, Group 2 and 3 are employed to complete this task in latter section.

Table 1: Regression results for group velocity identification (corresponding to Figure 4(a))

Group 1			Group 2			Group 3		
c_g (m/s)	c_g bound (m/s)	R^2	c_g (m/s)	c_g bound (m/s)	R^2	c_g (m/s)	c_g bound (m/s)	R^2
5308	[5258,5359]	0.99	5340	[5279,5402]	0.99	5291	[5257,5325]	0.99

Table 2: The regression results for attenuation coefficient identification (corresponding to Figure 4(b))

Group 1			Group 2			Group 3		
k_i (Np/m)	k_i bound (Np/m)	R^2	k_i (Np/m)	k_i bound (Np/m)	R^2	k_i (Np/m)	k_i bound (Np/m)	R^2
0.85	[0.66,1.04]	0.39	0.92	[0.81,1.03]	0.92	0.97	[0.80,1.13]	0.79

4.2.2 Identified dispersion curves of group velocity and attenuation coefficient

The group velocity and attenuation coefficient at each frequency can be identified by using the method shown in Figure 4(a) and (b) respectively. After that, the group velocity dispersion curves can be formed as shown in Figure 5(a), in which only the result of Group 1 is presented given that the three groups generate pretty close group velocity dispersion curves, and the attenuation coefficient dispersion curves are shown in Figure 5(b). Additionally, Figure 5(c) presents the respective correlation coefficients for group velocity and attenuation. There is no doubt that for group velocity identification all correlation coefficients are greater than 0.95. Hence the identified S0 mode group velocity dispersion curve is reliable.

From the attenuation coefficient dispersion curves (Figure 5(b)) and its corresponding correlation coefficients (Figure 5(c)), the following findings are observed. Firstly, both groups' curves present the same trend, i.e., attenuation increasing with frequency firstly and then decreasing. Secondly, the correlation coefficients of both groups at the initial several points (50-60kHz) are smaller than 0.6. This may be explained by tuning effect of Lamb wave, for which at the lower frequency range, the amplitude of S0 mode is too small to be easily extracted from experimental signals [15]. Finally, the correlation coefficient starts to diminish after 150kHz for both groups, which could be explained by the low sampling frequency and high frequency noise contamination. In later damping parameters estimation, only the identified attenuation coefficients of Group 3 in frequency range from 70kHz to 150kHz are used to be the training data when implementing Eq. (16).

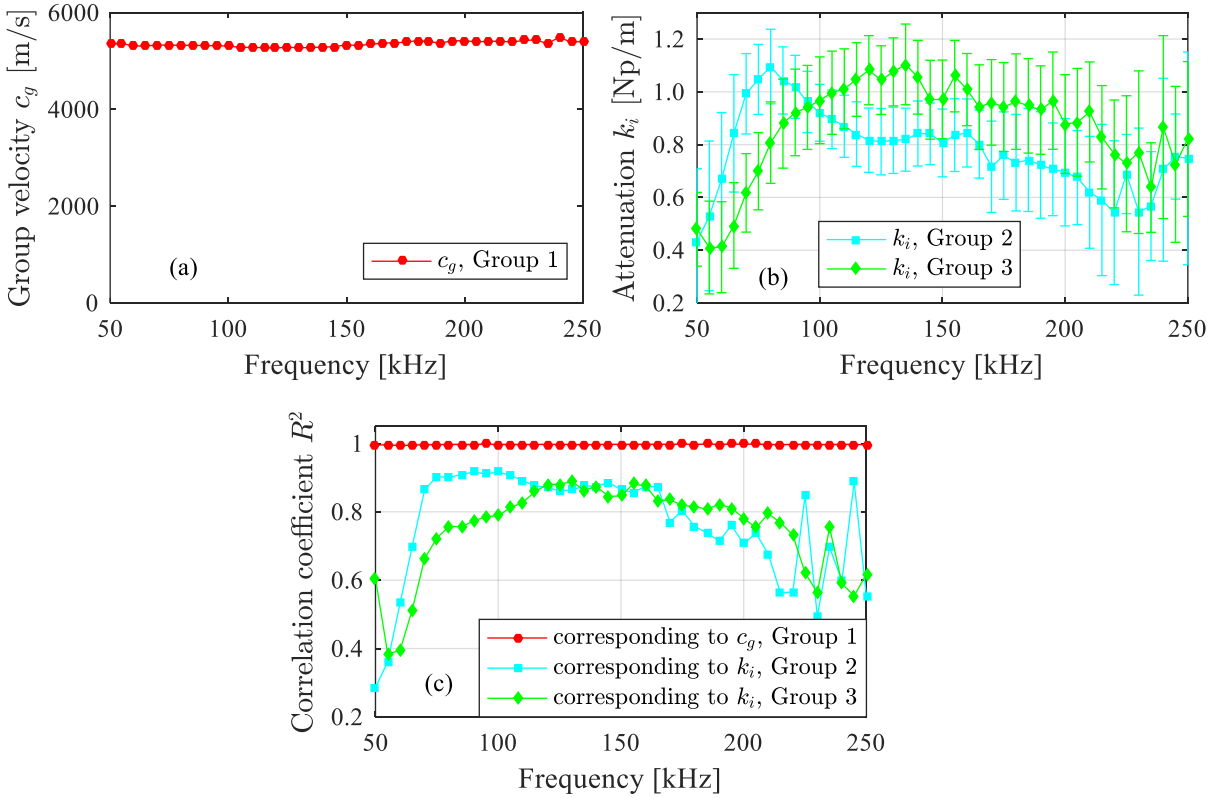

Figure 5: (a) the group velocity dispersion curve, (b) the attenuation coefficient dispersion curve and (c) correlation coefficient

4.3 Estimation of material properties

The experimentally identified dispersion curves of group velocity and attenuation coefficient are further employed to estimate the material properties via the least square method presented in section 3.2. Thus, the group velocity dispersion curve shown in Figure 5(a) is firstly adopted to estimate the storage modulus and Poisson ratio. The initial and optimal values of both parameters are listed in Table 3.

The calculated group velocity dispersion curves for S0 and A0 mode using the optimal value and the experimentally identified data points are depicted in Figure 6. It can be seen that the calculated S0 mode group velocity dispersion curve agrees well with the experiment. Besides, the calculated S0 mode phase velocity dispersion curve is provided as well in this figure which totally overlaps with the calculated group velocity dispersion curve in the frequency range. Comparing the calculated S0 and A0 mode group velocity dispersion curves, it is easy to infer that A0 mode Lamb wave propagates at approximately the half speed of S0 mode in the evaluated frequency range. Thus there is no any A0 mode group velocity can be identified from the experiment because of the abundant S0 mode wave reflections.

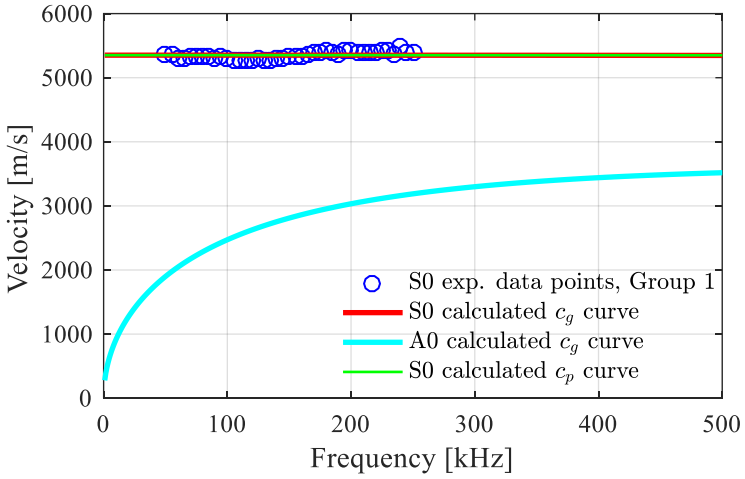

Figure 6: Comparison between the calculated and identified dispersion curve of group velocity

The experimentally identified attenuation coefficients are subsequently employed to estimate the damping parameters of the three damping models. The initial and optimal values are listed in Table 3, in which the optimal term γ_{KV} and ϵ do not change from its initial value, which is caused by accident.

Table 3: The estimated parameters of FCS

	E	ν	γ_{HR}	γ_{KV}	γ_{BT}	ϵ
Initial value	50GPa	0.2	0.03	0.03	0.03	10
Optimal value	44.4GPa	0.05	0.014	0.03	0.017	10

4.4 Attenuation coefficient prediction for a wide frequency range

All the required parameters are provided as inputs to the developed algorithm presented in Figure 1 and the attenuation coefficient for a wide frequency range is predicted as shown in Figure 7(a). The experimentally identified attenuation coefficient of Group 2 and 3 in the frequency range from 70kHz to 150kHz is provided as well for comparison. It can be seen that the predicted curves for HR and BT model agree well with the experimentally identified points with strictly linear trend. However, the curve of KV model presents the concave trend. Thanks to this reason, it is only suitable for predicting attenuation coefficient in a narrow frequency band for the current composite structure.

The developed numerical algorithm in Figure 1 is further used to predict the wavenumber which is extracted from the real part k_r of the complex solution as depicted in Figure 7(b). The identified wavenumber calculated via $k = \frac{\omega}{c_p}$ is also provided for comparison, in which c_p is replaced by c_g given that the approximated relation ($c_p \approx c_g$) from Figure 6. It can be seen that the theoretically calculated wavenumber dispersion curves for HR and KV model are consistent with the experimentally identified data points. But BT model predicts a minor smaller wavenumber in the evaluated frequency range than HR and KV model. The high coincidence between the predicted and identified wavenumber or group velocity reveals that the group velocity, phase velocity and wavenumber can be obtained more reliable from experiment or theoretical prediction than the attenuation coefficient.

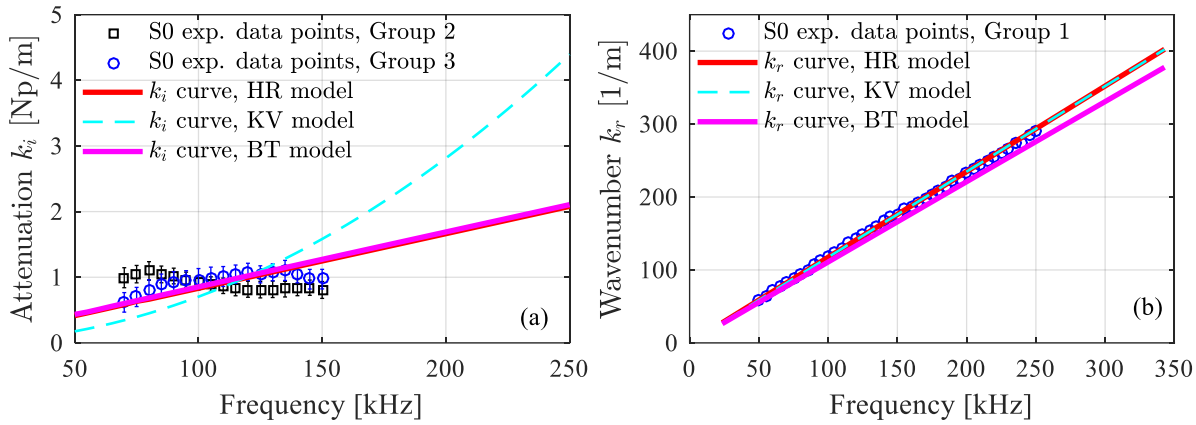

Figure 7: Prediction of (a) attenuation coefficient and (b) wavenumber at a wide frequency range

5 CONCLUSIONS

- In this article, a numerical algorithm to predict Lamb wave attenuation coefficient is proposed firstly. This algorithm is derived directly from dispersion equations by considering three damping models, HR, KV and BT model. The curve tracing technique is adopted to enhance the reliability of solving the complex equation.
- The linear regression method is used to identify group velocity and attenuation coefficient from experimentally measured Lamb wave signals. The least square formulation is designed for estimating the storage modulus and Poisson ratio of material as well as damping parameters of the three damping models.
- A comprehensive case study on a practical aeronautical structure validated that the

proposed attenuation coefficient prediction algorithm is feasible and effective. Comparing to group velocity, accurately identifying and predicting attenuation of Lamb wave in complex composite structures is more difficult and urgent. The presented outcomes in this article are an useful attempt.

REFERENCES

[1] Su Z and Ye L. Identification of Damage Using Lamb Waves. *Springer* (2009).

[2] Sohn, H., Farrar, C.R., Hemez, F.M., Shunk, D.D., Stinemates, D.W. and Nadler, B.R. A review of structural health monitoring literature: 1996–2001. *Los Alamos National Laboratory report* (2002).

[3] Wilcox, P., Lowe, M., and Cawley, P. The effect of dispersion on long-range inspection using ultrasonic guided waves. *NDT&E International* (2001) **34**:1-9.

[4] Manconi, E. and Sorokin, S. On the effect of damping on dispersion curves in plates. *International Journal of Solids and Structures* (2013) **50**:1966–1973.

[5] Neau, G. Lamb waves in anisotropic viscoelastic plates: study of the wave fronts and attenuation. PhD Thesis, University of Bordeaux I, France, 2003.

[6] Mei, H. and Giurgiutiu, V. Guided wave excitation and propagation in damped composite plates. *Structural Health Monitoring* (2018) **18**:690–714.

[7] Quintanilla, F.H., Fan, Z., Lowe, M.J.S. and Craster, R.V. Guided waves' dispersion curves in anisotropic viscoelastic single- and multi-layered media. *Proc. R. Soc. A* 471 (2183), 20150268.

[8] Ramadas, C., Balasubramaniam, K., Hood, A., Joshi, M. and Krishnamurthy, C.V. Modelling of attenuation of Lamb waves using Rayleigh damping: Numerical and experimental studies. *Composite Structures* (2011) **93**:2020–2025.

[9] Gresil, M. and Giurgiutiu, V. Prediction of attenuated guided waves propagation in carbon fiber composites using Rayleigh damping model. *Journal of Intelligent Material Systems and Structures* (2015) **26**:2151–2169.

[10] Wandowski, T., Kudela, P., Malinowski, P. and Ostachowicz, W. Guided wave attenuation in composite materials. *Proc. SPIE 10170, Health Monitoring of Structural and Biological Systems* (2017) 101701D.

[11] Rose, J.L. Ultrasonic Guided Waves in Solid Media. *Cambridge University Press* (2014).

[12] Mastroddi, F., Martarelli, F., Eugeni, M. and Riso, C. Time- and frequency-domain linear viscoelastic modeling of highly damped aerospace structures. *Mechanical Systems and Signal Processing* (2019) **122**:42–55.

[13] Lowe, M.J.S. Matrix Techniques for Modeling Ultrasonic Waves in Multilayered Media. *IEEE Transactions on Ultrasonics, Ferroelectrics, and Frequency Control* (1995) **42**:525-542.

[14] Lourakis, M.I. A Brief Description of the Levenberg-Marquardt Algorithm Implemented by levmar. (2005).

[15] Mei, H. and Giurgiutiu, V. Effect of structural damping on the tuning between piezoelectric wafer active sensors and Lamb waves. *Journal of Intelligent Material Systems and Structures* (2018) **29**:2177-2191.